PAPER

Check for updates

Near-UV light emitting diode with on-chip photocatalysts for purification applications†

Young-Chul Leem,[ab] NoSoung Myoung,[a] Sang-Hyun Hong,[bc] Sehee Jeong,[a] Okkyun Seo,[d] Seong-Ju Park,[be] Sang-Youp Yim [iD] *[a] and Joon Heon Kim [iD] *[a]

A new design for light-emitting diodes (LEDs) with on-chip photocatalysts is presented for purification applications. An array of disk-shaped TiO_2, with a diameter of several hundred nanometers, combined with SiO_2 pedestals was fabricated directly on the surface of an InGaN-based near-ultraviolet (UV) LED using a dry etching process. The high refractive-index contrast at the boundary and the circular shape can effectively confine the near-UV light generated from the LED through multiple internal reflections inside the TiO_2 nanodisks. Such a feature results in the enhancement of light absorption by the photocatalytic TiO_2. The degradation of the organic dye malachite green was monitored as a model photocatalytic reaction. The proposed structure of LEDs with TiO_2/SiO_2 nanodisk/pedestal array exhibited a photocatalytic activity that was three times higher than the activity of LEDs with a TiO_2 planar layer. The integration of photocatalytic materials with near-UV LEDs in a single system is promising for various purification applications, such as sterilization and disinfection.

Introduction

The demands of the lighting industry for new techniques have led to the development of devices with additional functions beyond high-efficiency lighting sources. Among them, light emitting diodes (LEDs) emitting ultraviolet (UV) light have emerged as one of the most promising technologies because they can be used for a variety of applications, such as polymer curing, insect induction, excitation of fluorescence, photo-therapy, medical imaging, sterilization, and disinfection.[1–3] Currently, the main application of UV lighting is polymer curing, which mostly requires near-UV light in the wavelength range of 365–400 nm. Near-UV LEDs, in particular InGaN-based LEDs, are a promising alternative for mercury-vapor lamps owing to their advantages, such as high energy efficiency, high sustainability, and environmental friendliness.[1]

Other important applications of UV light are sterilization and disinfection, mostly requiring deep-UV light in the

wavelength range of 250–280 nm.[4,5] AlGaN-based deep-UV LEDs can emit UV light in this wavelength range, but their use in industrial applications is limited. They present relatively low optical output owing to the strong absorption of UV light in the p-GaN layer resulting in low external quantum efficiency (∼7%). They also exhibit low injection efficiency and vulnerability of internal quantum efficiency to threading dislocations.[6–9] Furthermore, the widespread use of deep-UV light is restricted as the exposure of the human body to deep-UV radiation, even for a very short time, can cause severe health issues, such as keratoconjunctivitis or erythema. For example, the threshold energy for symptoms of photokeratitis is only 3.0 mJ cm^{-2} at a wavelength of 270 nm, whereas near-UV light of much higher energy is required to induce the same effect (4.7×10^4 mJ cm^{-2} at a wavelength of 380 nm).[10] Therefore, the safe use of LEDs is a factor as important as their optical performance for sterilizing/disinfecting applications and should be further examined.

For sterilization/disinfection applications, light can also be used indirectly to excite photocatalytic materials to generate highly reactive radicals, which can decompose toxic chemicals or biomaterials instead of light itself.[11,12] Among the various photocatalysts, TiO_2 is one of the most widely investigated compounds owing to its novel properties, such as non-toxicity, environmental-friendliness, biocompatibility, low-cost, and corrosion resistance.[13–15] Under near-UV illumination, TiO_2 can provide bactericidal action, water purification, and disinfection owing to its photocatalytic effect.[16–20] Therefore, a combination of TiO_2 and near-UV LED with an appropriate geometry for

[a] Advanced Photonics Research Institute, Gwangju Institute of Science and Technology, Gwangju 61005, Korea. E-mail: syim@gist.ac.kr; joonhkim@gist.ac.kr

[b] School of Materials Science and Engineering, Gwangju Institute of Science and Technology, Gwangju 61005, Korea

[c] GIST Central Research Facilities, Gwangju Institute of Science and Technology, Gwangju 61005, Korea

[d] Center for Synchrotron Radiation Research, Japan Synchrotron Radiation Research Institute (JASRI), 1-1-1, Kouto, Sayo, Hyogo 679-5198, Japan

[e] School of Energy Engineering, Korea Institute of Energy Technology, Naju, Jeonnam 58217, Korea. E-mail: sjpark@kentech.ac.kr

† Electronic supplementary information (ESI) available. See https://doi.org/10.1039/d2na00305h

inducing high photocatalytic efficiency is a promising strategy for purification applications.

In general, the absorption of UV photons by TiO_2 can induce an electron transition from the valence to the conduction band, accompanied by the creation of holes in the valence band. When excited carriers migrate to the surface of TiO_2 photocatalysts they can generate various reactive species, such as hydroxyl (OH) and hydroperoxyl (HO_2) radicals. These reactive species can initiate secondary reactions that decompose nearby organic materials leading to sterilization and purification.[13,18] Therefore, to enhance photocatalytic activity, light absorption by TiO_2, resulting in the generation of electron–hole pairs, should be increased. Meanwhile, the surface-to-volume ratio of the TiO_2 structure should be increased to facilitate the diffusion of the generated electrons and holes to the surface before they recombine inside TiO_2.[14] Therefore, to develop near-UV LEDs with excellent purifying characteristics, it is necessary to construct an optimal photocatalytic LED structure.

To enhance the surface-to-volume ratio of the TiO_2 structure on LEDs, an array of zero-dimensional TiO_2 nanostructures is preferable to a continuous two-dimensional TiO_2 film structure. For example, when the disk diameter is four times the disk thickness, a zero-dimensional TiO_2 nanodisk array can provide a surface-to-volume ratio two times higher than that of a two-dimensional TiO_2 film (ESI†).

To enhance light absorption by TiO_2, the light path length inside TiO_2 should be extended by effectively confining the light generated from the active layer of the LED inside the TiO_2 materials before its escape. However, previous studies on LEDs with various innovative shapes, such as textured surfaces, photonic crystals, and hierarchical structures, have mostly focused on improving light extraction rather than light trapping.[21–23]

The high refractive index of TiO_2 ($n \approx 3.1$) in the near-UV wavelength[24] is intrinsically advantageous; high-refractive-index materials surrounded by materials with a low refractive index, such as water ($n = 1.3$) and air ($n = 1$), can concentrate the light inside the material by preventing it from escaping for large incidence angle owing to the total internal reflection (TIR) at the boundary. In this regard, the introduction of a disk-shaped TiO_2 array onto a near-UV LED can be advantageous; the circular configuration of high-refractive-index materials effectively circulates the obliquely incident light via TIR at its side boundary before its escape, resulting in an extended light path length inside each TiO_2 nanodisk.[25,26] This increased UV absorption of TiO_2 enhances its photocatalytic activity for sterilization and purification.

Herein, we demonstrate the enhanced photocatalytic degradation of organic dyes by a TiO_2 nanodisk combined with a flip-chip-structured near-UV LED. The flip-chip structure, in which photons generated in active layers are emitted from the bottom side of the sapphire substrate, is a promising architecture for high-efficiency LEDs owing to its excellent heat dissipation capability, uniform current spreading, and elimination of light propagation hindrance due to bonding pads.[27] To fabricate a novel structure combining the TiO_2 nanodisk and the flip-chip near-UV LED, a self-assembled silica microsphere monolayer was used as an etching mask to produce the TiO_2 nanodisk array from the TiO_2 film on the sapphire surface of the near-UV LED.[23,28] Moreover, we fabricated a TiO_2 nanodisk array with SiO_2 pedestals on the sapphire surface of the near-UV LED. Since the refractive index of SiO_2 ($n = 1.47$) is smaller than that of sapphire ($n = 1.8$),[29] the enhanced refractive index contrast at the bottom of the TiO_2 nanodisk can further enhance the light-trapping efficiency of the material.

The TiO_2 nanodisk array with SiO_2 pedestals on the near-UV LED showed approximately three-fold higher activity in the photocatalytic degradation of malachite green (MG) than the flat TiO_2 layer on the same LED. The TiO_2 nanodisk array without SiO_2 pedestals presented 2.2 times higher activity than the flat TiO_2 layer. The optical absorption properties of these structures were experimentally studied using UV-visible (UV-vis) absorption spectroscopy and confocal scanning electroluminescence microscopy (CSEM). Theoretical studies were conducted via finite-difference time-domain (FDTD) electromagnetic simulation. All of these confirmed the effectiveness of the use of the TiO_2 nanodisk array, especially with SiO_2 pedestals, on the near-UV LED structure for photocatalytic applications.

Experimental

Fabrication of near-UV InGaN-based LEDs

Near-UV LEDs, with a dominant emission peak near 370 nm (Fig. S1†), were grown on a c-plane sapphire substrate via metal–organic chemical vapor deposition (MOCVD). After the growth of a 2.5 μm-thick undoped GaN buffer layer, a 2 μm-thick Si-doped n-GaN layer was grown at 1010 °C. Five pairs of InGaN/GaN multiple quantum wells (MQWs) were then grown, followed by a 110 nm-thick p-type GaN layer and a 25 nm-thick p-type AlGaN layer. To fabricate the flip-chip structured LEDs, the p-GaN and MQW layers were partially etched using inductively coupled plasma (ICP) etching until the n-GaN layer was exposed, and Cr/Au-based n-pad electrodes were deposited via electron beam evaporation. LEDs of 300 μm × 300 μm size were fabricated by depositing an Ag-based p-pad electrode on the p-GaN layer via electron beam evaporation (Fig. 1, inset).

Fabrication of TiO_2/SiO_2 nanodisk structures

Fig. 1 presents the manufacturing process of the disk-shaped TiO_2 photocatalytic layer with SiO_2 pedestals on the surface of a sapphire substrate, which is the opposite side of the GaN-based epitaxial layers of the flip-chip near-UV LED. First, a 200 nm-thick SiO_2 layer was grown on a sapphire substrate via plasma-enhanced chemical vapor deposition, and then a 200 nm-thick TiO_2 layer was deposited through electron beam evaporation. The amorphous TiO_2 thin film was annealed at 450 °C for 3 h in atmospheric pressure to convert TiO_2 to the anatase phase, which is known to provide the highest photocatalytic activity among the TiO_2 crystal structures. The surface of the TiO_2 thin film was pretreated with oxygen plasma for 5 min to reduce its surface energy and facilitate the dip-coating process of the two-dimensional (2D) colloidal layer. A hexagonal
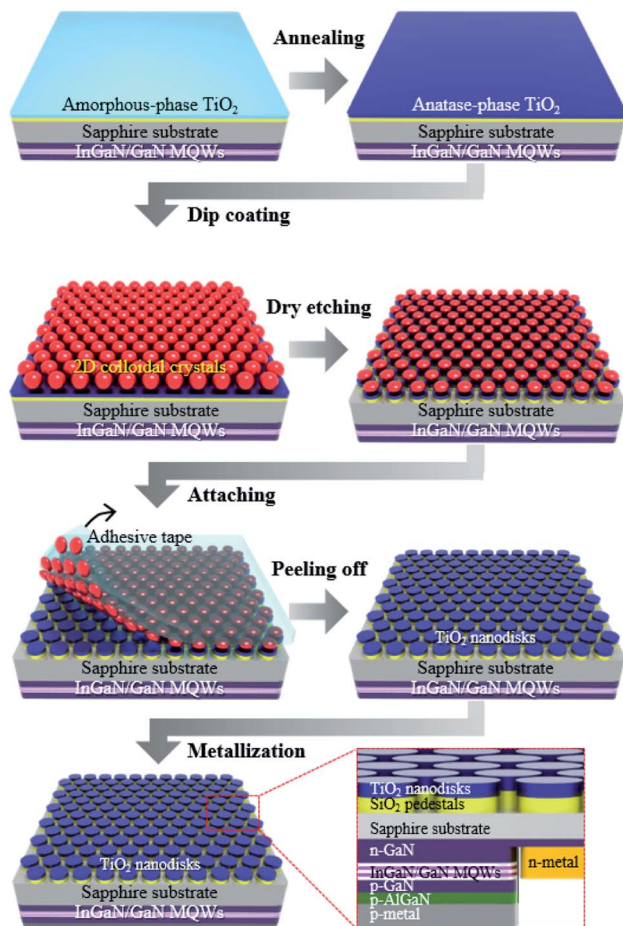
Fig. 1 Schematic of the fabrication steps of the TiO$_2$/SiO$_2$ nanodisk/pedestal array on the near-UV LED: Dip-coating for self-assembling the silica spheres (1 μm in diameter) on the TiO$_2$ layer; dry etching of the TiO$_2$/SiO$_2$ layer using the close-packed silica sphere monolayer as an etching mask; removal of the residual silica spheres using an adhesive tape; metallization to form p- and n-electrode metals. Inset illustrates the cross-sectional view of the final structure with the TiO$_2$/SiO$_2$ nanodisk/pedestal array on the near-UV LED.

close-packed (HCP) 2D colloidal crystal composed of 1 μm diameter silica spheres was deposited on the surface *via* dip-coating using 15 wt% of a silica colloidal suspension in ethanol.[23] Next, ICP etching, using the HCP silica monolayer as an etching mask, was conducted to form a hexagonal array of the disk-shaped TiO$_2$/SiO$_2$ layer with a diameter of 750 nm. After ICP etching, the residual silica spheres on the TiO$_2$/SiO$_2$ nanodisk array were gently removed by attaching and peeling the adhesive tape.

Optical measurements using UV-vis absorption spectroscopy and CSEM

The UV-vis absorption spectra of the TiO$_2$ nanodisk and the TiO$_2$/SiO$_2$ nanodisk/pedestal arrays fabricated on the sapphire substrate were measured in the transmission geometry using a PerkinElmer Lambda 900 UV/vis/NIR spectrophotometer. CSEM measurements were performed using a modified commercial confocal scanning microscope (WITec GmbH). The

electroluminescence (EL) light was collected from the samples using a microscope objective (×100, NA 0.9) and delivered to the detector (photomultiplier tube, PMT) *via* a multimode optical fiber (φ_{core} = 50 μm) for EL mapping. During the experiments, an injection current of 20 mA from a Keithley 2450 current source was applied to the LED. The spatial EL distribution for the 5×5 μm^2 region was obtained in 10 nm steps using a piezoelectric (PZT) nano-positioning stage.

Three-dimensional FDTD simulation

FDTD simulation was performed using a commercially available software (Lumerical FDTD Solutions) to investigate light propagation through the hierarchical surface structures of the LEDs. A point dipole source polarized along the y axis was located in the center of the MQWs to simulate light generated from the LED as transverse electric (TE) polarization was predominantly observed in InGaN/GaN MQW LEDs.[30–32] The point dipole source was assumed to emit monochromatic light with a wavelength of 370 nm. The simplified LED structure for the FDTD simulation was composed of a 100 nm-thick Ag mirror, 110 nm-thick p-GaN layer, 100 nm-thick InGaN/GaN MQW layer, 2 μm-thick n-GaN layer, 2.5 μm-thick undoped GaN layer, and 750 nm-diameter TiO$_2$/SiO$_2$ nanodisk. The model structure of the LED was surrounded by a perfectly matched layer (PML).[33]

Evaluation of the photocatalytic purifying activity

The photocatalytic purifying activity of the fabricated near-UV LEDs with TiO$_2$ nanodisks was evaluated by investigating the photocatalytic degradation of MG in water at room temperature.[34] A cylindrical cell with an inner diameter of 8 mm was built on top of the photocatalytic structure of the LED and was filled with a 100 μL aqueous MG solution with a concentration of 0.1 g L^{-1} (Fig. S2†). After waiting for 1 h in the dark to establish an adsorption/desorption equilibrium of MG on the photocatalytic layer, the near-UV LED was turned-on at an injection current of 20 mA to illuminate the photocatalytic layer on the LED surface by the near-UV LED light at a peak wavelength of 370 nm. During the photocatalytic degradation of MG in the aqueous solution, the reaction cell was covered with a glass to prevent the evaporation of the solution. The degradation rate of the MG solution was determined by the change in its concentration. To calculate the MG concentration, the absorbance of the solution was monitored in 30 min intervals using an optical microscope equipped with a collimated external LED light source with a nominal wavelength of 617 nm, which is close to the absorption peak of MG (Fig. S3†).

Results and discussion

Fig. 2a and b present the scanning electron microscope (SEM) images and a photograph (inset) of the homogeneous formation of the HCP 2D colloidal crystal of silica microspheres covering a large area on the TiO$_2$/SiO$_2$ layer grown on a sapphire substrate with a diameter of 2 inches. The photograph of the silica sphere monolayer shows green iridescence owing to the
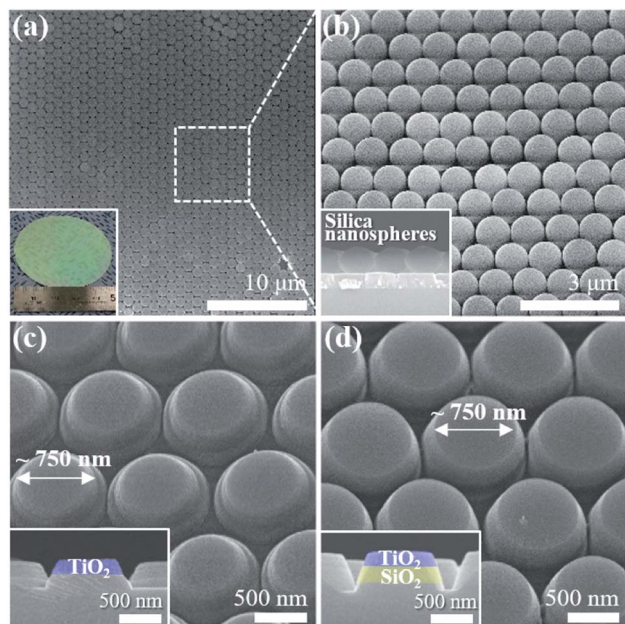
Fig. 2 (a) Two-dimensional colloidal crystal on a TiO_2/SiO_2 layer grown on a 2 inch-diameter sapphire substrate. (b) Top-view SEM image of the 2D hexagonal crystal of silica spheres with a diameter of 1 μm before ICP etching. Inset is the cross-sectional SEM image of the residual silica spheres on the TiO_2/SiO_2 nanodisk/pedestal array after ICP etching. SEM images with a 45°-inclined angle view of (c) pristine TiO_2 nanodisk array and (d) TiO_2/SiO_2 nanodisk/pedestal array. Insets are the corresponding cross-sectional SEM images of nanodisks.

constructive interference of visible light by the ordered colloidal crystal, which is similar to the photonic crystal. The top-view SEM images of the HCP 2D colloidal crystal clearly show the long-range ordering of silica spheres. The inset of Fig. 2b represents a cross-sectional SEM image of the residual silica spheres together with the etched TiO_2/SiO_2 layer after the ICP etching.

As the ICP etching progressed, the pristine TiO_2 nanodisk array on the sapphire substrate formed below the silica sphere layers with a concomitant reduction in the size of each silica sphere (Fig. 2). By changing the ICP etching time, the diameter of nanodisks can be controlled (Fig. S4†). Fig. 2c and d show the bird's-eye view SEM images of the TiO_2 nanodisks and the TiO_2 nanodisks with SiO_2 pedestals with a diameter of 750 nm, respectively. These nanodisks were used for following experiments.

The current–voltage (I–V) characteristics of the near-UV LEDs with different structures (planar TiO_2 film, TiO_2 nanodisk array, and TiO_2/SiO_2 nanodisk/pedestal array) show similar forward voltages of 3.46–3.48 V, as shown in Fig. S5.† The identical I–V characteristic curves of the LEDs with the four different surface structures indicate that the fabrication process of TiO_2 nanodisks, including ICP etching and annealing to convert TiO_2 from the amorphous to the anatase phase, does not affect the electrical properties of the LEDs.

To investigate the crystal properties of the TiO_2 nanodisks, we performed X-ray diffraction (XRD) measurements using the 5D GIST beamline of the Pohang Light Source (PLS) in Korea.

The X-ray energy was set at 10 keV (1.24 Å) using a double-bounced Si (111) monochromator (ESI, Fig. S6†). The XRD profiles of the TiO_2 films with and without the annealing process at 450 °C for the substrate's normal direction are shown in Fig. 3. The XRD profiles of these two structures commonly show a predominant sapphire (0006) diffraction peak at 33.27°. The XRD profile of the annealed TiO_2 film clearly showed peaks corresponding to the anatase phase of the TiO_2 crystal planes of (101), (004), (200), (105), (211), (213), (220), and (215) with lattice constants of $a = b = 3.78$ Å and $c = 9.49$ Å (JCPDS PDF #00-064-0863). The TiO_2 film without annealing showed no significant peaks related to the TiO_2 crystal phase.

To investigate the optical properties of the TiO_2 and TiO_2/SiO_2 nanodisk structures, their absorption spectra were compared with those of the film structures using a UV-vis absorption spectrometer (Fig. 4). As the wavelength decreased, the absorption rapidly increased from approximately 390 nm for both the planar TiO_2 and TiO_2/SiO_2 films. This value corresponds to the band gap energy of 3.2 eV, which is a characteristic of TiO_2.[14] However, the absorbance in the wavelength range of 365–400 nm corresponding to the near-UV light from the InGaN LED is much weaker compared to that at shorter wavelengths. Therefore, to enhance the photocatalytic efficiency of the InGaN LED, it is necessary to increase the absorption by extending the light path length through alterations in the structure of the TiO_2 layer.

As shown in Fig. 4, the TiO_2 and TiO_2/SiO_2 nanodisk array structures presented much higher absorbance values than the planar TiO_2 and TiO_2/SiO_2 films in the wavelength range of the near-UV light (365–400 nm) from the InGaN LED. The increased absorbance of the nanodisk array can be attributed to the increased scattering as well as the extended path length of the light inside the TiO_2 nanodisks through TIR. In contrast to the planar layer, the nanodisk array can significantly scatter incident light, and part of the obliquely scattered light can be re-absorbed by the nearby nanodisks. Once the light is injected
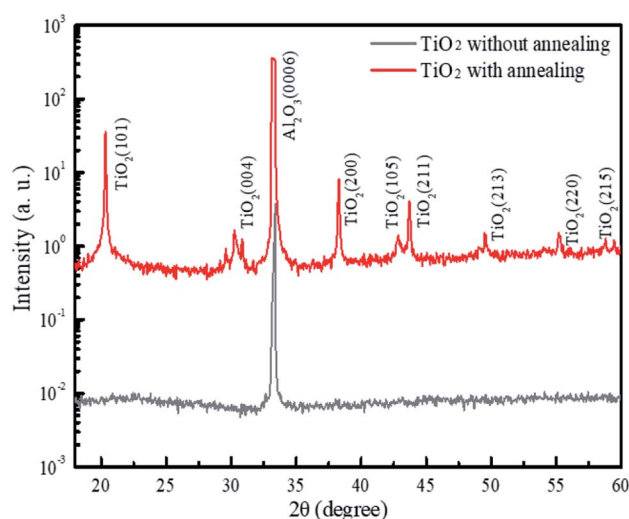

Fig. 3 XRD patterns of the TiO_2 film on the sapphire substrate with and without annealing at 450 °C for 3 h.
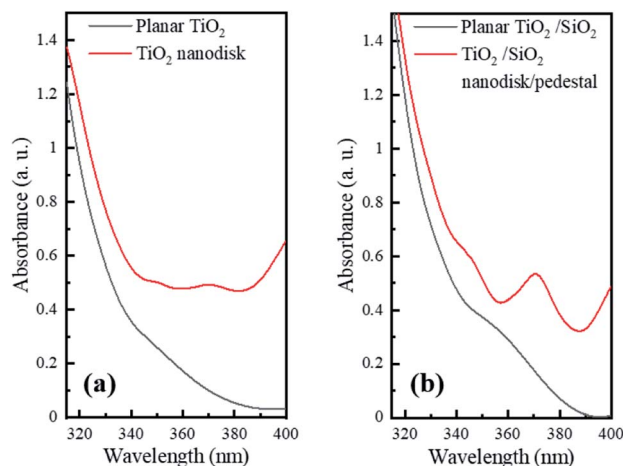
© 2022 The Author(s). Published by the Royal Society of Chemistry

Fig. 4 UV-vis absorption spectra of (a) pristine TiO_2 nanodisks and (b) TiO_2 nanodisks on SiO_2 pedestals compared to their planar films.

into the TiO_2 nanodisk, the high refractive index contrast between TiO_2 ($n = 3.1$ for 370 nm)[24] and air ($n = 1$) at the TiO_2/air boundary can be advantageous in reducing the light escaping from the side edge as well as the top plane of the nanodisk *via* TIR. In addition, the circular shape of the TiO_2 nanodisk is beneficial for circulating light inside the structure through multiple internal reflections at its circumference.

Fig. 5 shows the photocatalytic degradation of MG as a function of the LED operating time for various TiO_2-based surface configurations, such as the planar TiO_2 film, TiO_2 nanodisk array, and TiO_2/SiO_2 nanodisk/pedestal array. The time-dependent change of the MG concentration shows a typical single-exponential decay curve whose rate is different for various TiO_2 structures. To compare the degradation rate of each structure, the ln-linear plot of the MG concentration *versus* time was fitted to the following equation:

$$\ln C - \ln C_0 = -kt \tag{1}$$

where C and C_0 are the concentration at time t and the initial concentration of MG, respectively, and k is the apparent degradation rate constant. The values of k were obtained from the slopes of the fitting lines for $\ln(C/C_0)$ *vs.* t plots, as indicated by the dashed lines in Fig. 5.

In the absence of TiO_2, the MG concentration did not change, which confirms that the near-UV light at approximately 370 nm cannot directly degrade MG molecules under the experimental conditions. When the near-UV light illuminated TiO_2, MG was drastically degraded, with the degradation rate being different for different TiO_2 structures. The measured degradation rates of the LEDs with the planar TiO_2 film, TiO_2 nanodisk array, and TiO_2/SiO_2 nanodisk/pedestal array were 0.010, 0.022, and 0.030 min^{-1}, respectively. The TiO_2/SiO_2 nanodisk/pedestal array exhibited three and 1.4 times higher photocatalytic activity than the planar TiO_2 layer and the TiO_2 nanodisk array without SiO_2 pedestals, respectively. The higher photocatalytic activity of the TiO_2/SiO_2 nanodisk/pedestal array compared to that of other structures should be related to the more confinement and absorption of near-UV light inside TiO_2.

The optical properties of the nanodisk structures were examined by performing three-dimensional FDTD simulations at 370 nm (the peak wavelength of our InGaN-based near-UV LED), for the TiO_2 and TiO_2/SiO_2 nanodisks (Fig. 6). Fig. 6a–d show the electric field distribution in the TiO_2 and TiO_2/SiO_2 nanodisk structures when light from the LED is obliquely incident on the TiO_2 nanodisks. The very high intensity inside the TiO_2 nanodisk compared to that outside it clearly shows the effective confinement of light inside the TiO_2 nanodisk. In addition, the formation of strong modes around the circumference is clear in the TiO_2/SiO_2 nanodisk/pedestal structure (Fig. 6c), while the modes are slightly weaker in the TiO_2 nanodisk without the SiO_2 pedestal structure (Fig. 6a).

The modes along the circumference indicate that the light inside the TiO_2 nanodisk can be repetitively reflected at its
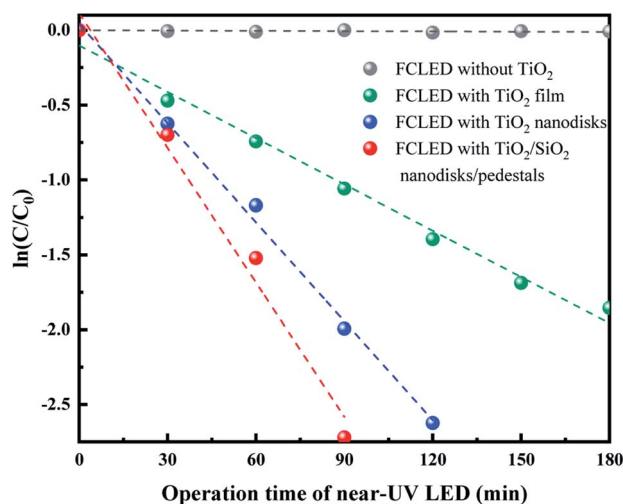

Fig. 5 Photocatalytic degradation of MG as a function of the operation time of LEDs for the planar TiO_2 film, TiO_2 nanodisk array, and TiO_2/SiO_2 nanodisk/pedestal array. Each dashed line presents the linear fitting for the measured data.
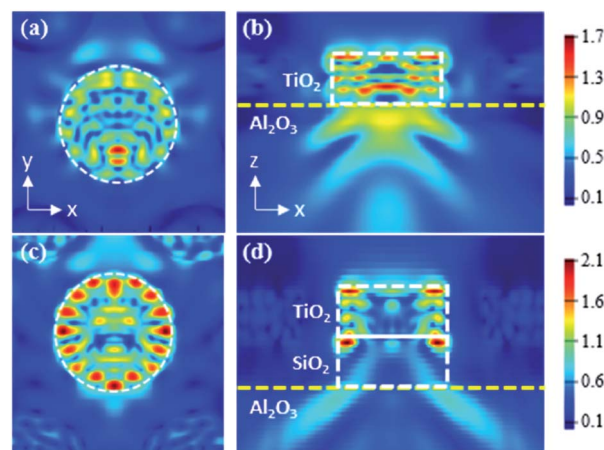

Fig. 6 Simulated electric field distribution in the $x-y$ plane and the cross-sectional ($x-z$) plane of (a and b) pristine TiO_2 nanodisk and (c and d) TiO_2/SiO_2 nanodisk/pedestal. Dashed lines indicate the position of the nanodisk.

circular boundary without significant escape. During multiple internal reflections, light can be greatly absorbed by TiO$_2$ to enhance a photocatalytic effect. The escape of light from the top plane of the TiO$_2$ nanodisk was not significant, mostly because of the high refractive index contrast at the TiO$_2$/air boundary (3.1/1.0). For this refractive index contrast, all the incident light from the TiO$_2$ side at an incident angle larger than the TIR critical angle of 19° should be totally reflected.

The TIR effect on the confinement of light worked in a similar way for the bottom plane of the TiO$_2$ nanodisk. However, the confinement effect of light inside TiO$_2$ at the bottom plane should be weaker than that of the top plane owing to the smaller refractive index contrast at the TiO$_2$/sapphire boundary (3.1/1.8), for which the TIR critical angle is 35°. In this regard, the use of a SiO$_2$ layer ($n = 1.47$) between TiO$_2$ and sapphire, whose refractive index is smaller than that of sapphire ($n = 1.8$), can further reduce the lower-direction escape of light from the TiO$_2$ nanodisk at the bottom side. Such a layer can increase the refractive index contrast at the bottom plane of the TiO$_2$ nanodisk (TIR angle = 28°), although the coupling efficiency from the LED to the TiO$_2$ nanodisk can be concomitantly decreased.

Furthermore, the double height of the TiO$_2$/SiO$_2$ nanodisk/pedestal structure compared to that of the TiO$_2$ nanodisk can be advantageous for the re-absorption of the light escaping from the side edge of the nanodisk by the neighboring nanodisks. All these factors contribute to the enhanced photocatalytic activity of the TiO$_2$/SiO$_2$ nanodisk/pedestal structure.

The intensity of the light escaping from the TiO$_2$ nanodisk and TiO$_2$/SiO$_2$ nanodisk/pedestal arrays was experimentally measured *via* CSEM (Fig. 7) to compare the light confinement effects. As expected, the intensity of the light that escaped from the circular edge of the TiO$_2$ nanodisk was much lower than that escaping from the central part of the top plane of the nanodisk. During multiple reflections of light between the bottom and top disk planes of the TiO$_2$ nanodisk, the vertically incident light on its surface, mostly at the central part of the plane, can be partially transmitted. This possibly occurs owing to the low incident angle, despite the high refractive index contrast between TiO$_2$ and air. However, the reflectance at the TiO$_2$/air boundary is approximately 26% even under normal incidence conditions, which implies that a substantial amount of light can be reflected back to the inside of the structure, even

for a very small incident angle. For larger incident angles, the reflectance can be significantly increased. A comparison of Fig. 7a and b shows that the intensity of the light escaping from the TiO$_2$/SiO$_2$ nanodisk/pedestal array was weaker than that of the TiO$_2$ nanodisk array for the same injection current. This finding indicates that the TiO$_2$/SiO$_2$ nanodisk/pedestal array is more effective in confining the LED light in their nanostructures than the TiO$_2$ nanodisk array, as expected.

Conclusions

In summary, we demonstrated a new type of light source for photocatalytic purification applications by directly fabricating anatase-phase TiO$_2$ nanostructures on the surface of an InGaN-based near-UV LED. A TiO$_2$ nanodisk array with SiO$_2$ pedestals has been proposed as an effective structure for maximizing the light-trapping efficiency and surface-to-volume ratio of the TiO$_2$ layer. The high refractive index contrast and the circular shape of the boundary, which were advantageous for multiple reflections, resulted in strong optical confinement. This increased the effective absorption of the near-UV light by TiO$_2$, resulting in a high photocatalytic activity. The photocatalytic activity of this structure in degrading MG was approximately three times higher than that of the planar TiO$_2$ film when combined with the near-UV LED. In conclusion, it is expected that this study can provide a guideline for the design of integrated photocatalytic materials and LEDs in a single system for various purification applications, such as sterilization and disinfection.

Author contributions

Young-Chul Leem: conceptualization, methodology, investigation, formal analysis, writing – original draft. NoSoung Myoung: investigation. Sang-Hyun Hong: software. Sehee Jeong: investigation. Okkyun Seo: investigation. Seong-Ju Park: conceptualization, resources, writing – review & editing. Sang-Youp Yim: conceptualization, formal analysis, writing – review & editing. Joon Heon Kim: conceptualization, methodology, supervision, writing – review & editing.

Conflicts of interest

There are no conflicts to declare.

Acknowledgements

References

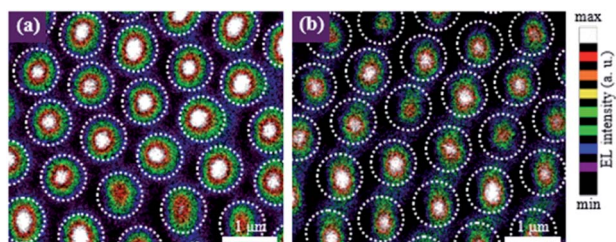1 Y. Muramoto, M. Kimura and S. Nouda, *Semicond. Sci. Technol.*, 2014, **29**, 084004.

Fig. 7 Experimental CSEM images of (a) TiO$_2$ nanodisk array and (b) TiO$_2$/SiO$_2$ nanodisk/pedestal array on the near–UV LED at an injection current of 20 mA. Circular dashed lines indicate the position of nanodisks.

2 K. Song, M. Mohseni and F. Taghipour, *Water Res.*, 2016, **94**, 341–349.

3 N. G. Yeh, C. H. Wu and T. C. Cheng, *Renewable Sustainable Energy Rev.*, 2010, **14**, 2161–2166.

4 T. Bintsis, E. Litopoulou-Tzanetaki and R. K. Robinson, *J. Sci. Food Agric.*, 2000, **80**, 637–645.

5 J. Chen, S. Loeb and J. H. Kim, *Environ. Sci.: Water Res. Technol.*, 2017, **3**, 188–202.

6 D. Y. Kim, J. H. Park, J. W. Lee, S. Hwang, S. J. Oh, J. Kim, C. Sone, E. F. Schubert and J. K. Kim, *Light: Sci. Appl.*, 2015, **4**, e263.

7 H. Hirayama, N. Maeda, S. Fujikawa, S. Toyoda and N. Kamata, *Jpn. J. Appl. Phys.*, 2014, **53**, 100209.

8 K. Ban, J. I. Yamamoto, K. Takeda, K. Ide, M. Iwaya, T. Takeuchi, S. Kamiyama, I. Akasaki and H. Amano, *Appl. Phys. Express*, 2011, **4**, 052101.

9 Y. Kuo, C. Y. Su, C. Hsieh, W. Y. Chang, C. A. Huang, Y. W. Kiang and C. C. Yang, *Opt. Lett.*, 2015, **40**, 4229–4232.

10 *Ultraviolet Radiation Guide*, Navy Environmental Health Center, Norfolk, Virginia, 1992.

11 J. M. Herrmann, *Catal. Today*, 1999, **53**, 115–129.

12 M. R. Hoffmann, S. T. Martin, W. Choi and D. W. Bahnemann, *Chem. Rev.*, 1995, **95**, 69–96.

13 J. Schneider, M. Matsuoka, M. Takeuchi, J. Zhang, Y. Horiuchi, M. Anpo and D. W. Bahnemann, *Chem. Rev.*, 2014, **114**, 9919–9986.

14 K. Nakata and A. Fujishima, *J. Photochem. Photobiol., C*, 2012, **13**, 169–189.

15 K. P. Gopinath, N. V. Madhav, A. Krishnan, R. Malolan and G. Rangarajan, *J. Environ. Manage.*, 2020, **270**, 110906.

16 D. Gumy, C. Morais, P. Bowen, C. Pulgarin, S. Giraldo, R. Hajdu and J. Kiwi, *Appl. Catal., B*, 2006, **63**, 76–84.

17 M. Cho, H. Chung, W. Choi and J. Yoon, *Water Res.*, 2004, **38**, 1069–1077.

18 A. Fujishima, T. N. Rao and D. A. Tryk, *J. Photochem. Photobiol., C*, 2000, **1**, 1–21.

19 D. Bertagna Silva, G. Buttiglieri and S. Babić, *Environ. Sci. Pollut. Res.*, 2021, **28**, 103–120.

20 T. S. Natarajan, M. Thomas, K. Natarajan, H. C. Bajaj and R. J. Tayade, *Chem. Eng. J.*, 2011, **169**, 126–134.

21 J. J. Wierer Jr, A. David and M. M. Megens, *Nat. Photonics*, 2009, **3**, 163–169.

22 W. C. H. Choy, W. K. Chan and Y. Yuan, *Adv. Mater.*, 2014, **26**, 5368–5399.

23 Y. C. Leem, J. S. Park, J. H. Kim, N. Myoung, S. Y. Yim, S. Jeong, W. Lim, S. T. Kim and S. J. Park, *Small*, 2016, **12**, 161–168.

24 A. Bendavid and P. J. Martin, *J. Aust. Ceram. Soc.*, 2014, **50**, 86–101.

25 S. Yang, Y. Wang and H. D. Sun, *Adv. Opt. Mater.*, 2015, **3**, 1136–1162.

26 J. Park, S. K. Ozdemir, F. Monifi, T. Chadha, S. H. Huang, P. Biswas and L. Yang, *Adv. Opt. Mater.*, 2014, **2**, 711–717.

27 J. J. Wierer, D. A. Steigerwald, M. R. Krames, J. J. O'Shea, M. J. Ludowise, G. Christenson, Y. C. Shen, C. Lowery, P. S. Martin, S. Subramanya, W. Götz, N. F. Gardner, R. S. Kern and S. A. Stockman, *Appl. Phys. Lett.*, 2001, **78**, 3379–3381.

28 L. Han, T. A. Piedimonte and H. Zhao, *Opt. Mater. Express*, 2013, **3**, 1093–1100.

29 M. J. Dodge, *Handbook of Laser Science and Technology, Volume IV, Optical Materials: Part 2*, CRC Press, Boca Raton, 1986.

30 K. B. Nam, J. Li, M. L. Nakarmi, J. Y. Lin and H. X. Jiang, *Appl. Phys. Lett.*, 2004, **84**, 5264–5266.

31 A. David, C. Meier, R. Sharma, F. S. Diana, S. P. Denbaars, E. Hu, S. Nakamura, C. Weisbuch and H. Benisty, *Appl. Phys. Lett.*, 2005, **87**, 101107.

32 J. Shakya, K. Knabe, K. H. Kim, J. Li, J. Y. Lin and H. X. Jiang, *Appl. Phys. Lett.*, 2005, **86**, 091107.

33 J. P. Berenger, *J. Comput. Phys.*, 1994, **114**, 185–200.

34 K. Natarajan, T. S. Natarajan, H. C. Bajaj and R. J. Tayade, *Chem. Eng. J.*, 2011, **178**, 40–49.